



Article

Electrochemical Study of $\text{Na}_2\text{Fe}_{1-x}\text{Mn}_x\text{P}_2\text{O}_7$ ($x = 0, 0.25, 0.5, 0.75, 1$) as Cathode Material for Rechargeable Na-Ion Batteries

Cristina Tealdi *, Monica Ricci, Chiara Ferrara, Giovanna Bruni, Eliana Quartarone and Piercarlo Mustarelli

Received: 30 September 2015; Accepted: 8 January 2016; Published: 15 January 2016

Academic Editor: Joeri Van Mierlo

Department of Chemistry, University of Pavia and INSTM, Viale Taramelli 16, 27100 Pavia, Italy;
ricci.monica15@gmail.com (M.R.); chiara.ferrara01@universitadipavia.it (C.F.); giovanna.bruni@unipv.it (G.B.);
eliana.quartarone@unipv.it (E.Q.); piercarlo.mustarelli@unipv.it (P.M.)

* Correspondence: cristina.tealdi@unipv.it; Tel.: +39-382-987-569; Fax: +39-382-987-575

Abstract: Sodium-ion batteries (SIBs) are considered a good choice for post-lithium devices. Transition metal sodium pyrophosphates are among the most interesting cathode materials for SIBs. Here we study the electrochemical properties of the system $\text{Na}_2\text{Fe}_{1-x}\text{Mn}_x\text{P}_2\text{O}_7$ ($x = 0, 0.25, 0.5, 0.75, 1$). By means of cyclic voltammetry (CV) and galvanostatic experiments, we confirm that pure Fe and Fe-rich compounds are promising for application in sodium batteries, whereas Mn-rich samples are less satisfactory, at least in case of solid-state reaction recipes and standard slurry preparations. Proper carbon coating is likely needed to improve the electrochemical behavior of Mn-rich samples.

Keywords: sodium batteries; cathode; pyrophosphate; structure; rate capability

1. Introduction

The improvement in the performances of secondary batteries attracts a great deal of attention, both in the portable and stationary applications market. The technological aspects bring along an increasing demand for materials optimization in terms of faster charge/discharge and capacity retention over prolonged usage. In addition, metal ion alternatives to Li for use in room temperature rechargeable batteries are currently under intense investigation and, in this context, Na-ion battery materials, in particular cathode materials, are the subject of a growing research interest [1–6]. Among the cathode materials currently proposed for use in Na-ion batteries, one of the most interesting is the family of two-sodium metal pyrophosphates of the general formula $\text{Na}_2\text{MP}_2\text{O}_7$ (M = Co, Cu, Fe, Mn) [7]. Such materials are known to crystallize in different polymorphic forms and, depending on the metal ion and the synthetic conditions, triclinic, monoclinic, orthorhombic or tetragonal structures have been reported [8–11]. $\text{Na}_2\text{FeP}_2\text{O}_7$ and $\text{Na}_2\text{MnP}_2\text{O}_7$ can be considered isostructural, crystallizing in the *P*-1 space group at room temperature [12]. In particular, among the possible polymorphs reported in the literature, this structure seems to be the most likely for the $\text{Na}_2\text{MnP}_2\text{O}_7$ composition when prepared by solid-state reaction under reducing conditions [13]. As shown in Figure 1, for both compounds the metal ions (Fe or Mn) occupy two crystallographic sites in the distorted octahedral environment. The $(\text{Fe},\text{Mn})\text{O}_6$ units are corner-shared and, together with P_2O_7 units, they form a three-dimensional framework with open channels, running parallel to the *a* axis, where the Na ions are positioned. While the metal-polyanion framework is essentially equivalent for the two compositions, a major difference between the two compounds has been identified in the number and relative occupancy of the Na sites. In particular, in $\text{Na}_2\text{FeP}_2\text{O}_7$ six distinct Na sites are present, with five of them being partially occupied [14], while in $\text{Na}_2\text{MnP}_2\text{O}_7$ Na sites are characterized by full occupancy [12]. Such a

structural difference may be among the causes at the basis of a different electrochemical activity for the two polymorphs.

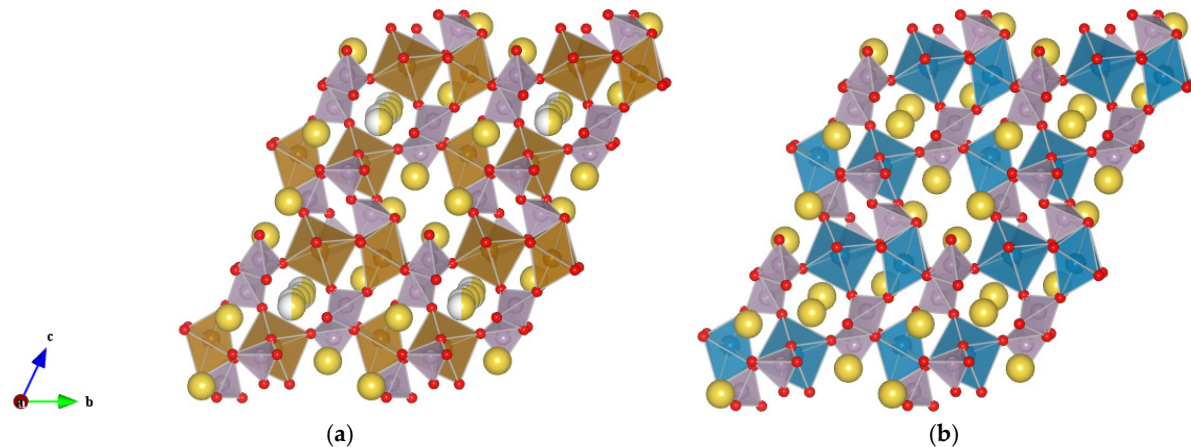


Figure 1. Schematic representation of the triclinic (space group $P-1$) (a) $\text{Na}_2\text{FeP}_2\text{O}_7$ and (b) $\text{Na}_2\text{MnP}_2\text{O}_7$ compounds. Partial occupancy on the Na sites is indicated by presence of two colors (yellow/grey) on the same sphere. Fe octahedra in brown, Mn octahedra in blue, and P tetrahedral in violet.

The theoretical capacity of $\text{Na}_2\text{FeP}_2\text{O}_7$, based on the one-electron process, is $97 \text{ mAh} \cdot \text{g}^{-1}$. Since the first reports, the electrochemical properties of $\text{Na}_2\text{FeP}_2\text{O}_7$ were described as highly promising, exhibiting a clear electrochemical activity in the potential range of 2–4.5 V *versus* Na/Na^+ with a reversible capacity of almost $90 \text{ mAh} \cdot \text{g}^{-1}$ at C/20 [15,16]. High reversible capacities of approximately $90 \text{ mAh} \cdot \text{g}^{-1}$ were found for this composition, in combination with ionic liquid electrolytes [17] and aqueous electrolytes [18]. Good capacity values, just below $80 \text{ mAh} \cdot \text{g}^{-1}$, were shown to be retained also at 1C rate [15] and improve when carbon-based nanocomposites are prepared [19]. The properties of $\text{Na}_2\text{MnP}_2\text{O}_7$ are more controversial, since either promising, approaching a reversible capacity of $80 \text{ mAh} \cdot \text{g}^{-1}$, [13,20] or very limited [12] electrochemical activity has been reported for this compound. In particular, a previous experimental study deals with the structural and magnetic characterization of the $\text{Na}_2\text{Fe}_{1-x}\text{Mn}_x\text{P}_2\text{O}_7$ series of compounds. The electrochemical investigation was restricted to a slow charge/discharge rate of C/20, but the study showed that, under these conditions, the electrochemical properties of the samples within this series were dramatically affected by the Fe/Mn substitution, with the activity of pure $\text{Na}_2\text{MnP}_2\text{O}_7$ being barely observable [12]. In this study we reinvestigate the $\text{Na}_2\text{Fe}_{1-x}\text{Mn}_x\text{P}_2\text{O}_7$ series, presenting electrochemical data related to a charge/discharge rate up to C/5, and discuss the results in view of the morphological characteristics of these compounds.

2. Experimental Section

Powder samples of nominal composition $\text{Na}_2\text{Fe}_{1-x}\text{Mn}_x\text{P}_2\text{O}_7$ ($x = 0, 0.25, 0.5, 0.75, 1$) were prepared by solid-state reaction starting from stoichiometric mixtures of $\text{Fe}(\text{C}_2\text{O}_4)_2 \cdot 2\text{H}_2\text{O}$ (Sigma-Aldrich, St. Luis, MO, USA, 99%), MnCH_3COOH (Sigma-Aldrich, 99%) and NaH_2PO_4 (Sigma-Aldrich, 98%). The reagents were thoroughly mixed in acetone and treated at 300°C for 3 h under steady Ar flow. After being reground and pelletized, the powers underwent a final thermal treatment at 600°C for 6 h (heating/cooling rate $5^\circ\text{C}/\text{min}$). In order to reach the completion of the synthesis, for the $\text{Na}_2\text{MnP}_2\text{O}_7$ composition a further treatment at 700°C for 3 h was necessary. All the thermal treatments were performed under Ar flow.

Phase purity was checked by means of X-ray powder diffraction (XRPD) measurements collected at ambient temperature through the use of a Bruker D8 Advanced powder diffractometer (Bruker, Billerica, MA, USA) operating in Bragg-Brentano geometry ($\text{Cu K}\alpha$ wavelength). Data were analyzed

according to the “Profile matching” procedure (Le Bail fitting) [21] to derive cell parameters and unit cell volume using the FullProf software [22].

Scanning electron microscope (SEM) measurements and energy dispersive microanalysis (SEM-EDS) were performed using a Zeiss EVO MA10 microscope (Zeiss, Oberkochen, Germany) coupled with an EDS detector (X-max 50 mm²).

For the electrochemical tests, the cathode slurry was prepared by mixing in a planetary milling (Fritsch, Pulverizette 7, Idar-Oberstein, Germany) for 10 min at 300 rpm the active material, carbon black (Alpha Aesar, Ward Hill, MA, USA, 99.9%) and PVdF in the ratio 70:20:10. The mixed powders were then dissolved in the minimum amount of *N,N*-methyl-pyrrolidone (Sigma-Aldrich, 99%) and kept under continuous stirring for 3 h. The slurry was casted onto an Al foil and heated at 100 °C for 1 h under vacuum to remove the organic solvent and subsequently cut in disks of 1 cm in diameter. Swagelok-type cells were assembled in an Ar-filled glove box using a cathode disk as working electrode, Na metal foil as counter and reference electrodes, Whatman disks as separators and NaPF₆ (Sigma-Aldrich, 98%) in a 0.5 M solution of anhydrous polycarbonate (PC) as the electrolyte.

Cyclic voltammetry (CV) measurements were collected using an Autolab PGSTAT30 Echo Chemie (Metrohm Autolab, Utrecht, The Netherlands) in the range 1.5–4.0 V versus Na/Na⁺ at a scan rate of 0.1 mV·s⁻¹ starting from open circuit voltage (OCV) conditions. Galvanostatic cycling tests were performed using an Arbin battery cycler (Model BT-2000, Arbin, College Station, TX, USA) in the range 1.5–4.0 V. All the cells were tested at room temperature.

3. Results and Discussion

Figure 2 shows the XRPD patterns of the Na₂Fe_{1-x}Mn_xP₂O₇ series. The diffraction patterns are in agreement with those previously reported for these compositions and they can be indexed according to the triclinic *P*-1 space group [12]. These results show that, as expected, the similarity between Fe and Mn facilitates the formation of a solid solution of nominal composition Na₂Fe_{1-x}Mn_xP₂O₇ in the whole compositional range. As shown in the Introduction (Figure 1), the two end-members, Na₂FeP₂O₇ and Na₂MnP₂O₇, can indeed be considered isostructural since the rigid framework constituted by (Fe,Mn)O₆ and PO₄³⁻ units is substantially equivalent, the major difference between the two compounds being identified in the number and relative occupancy of the Na sites [12].

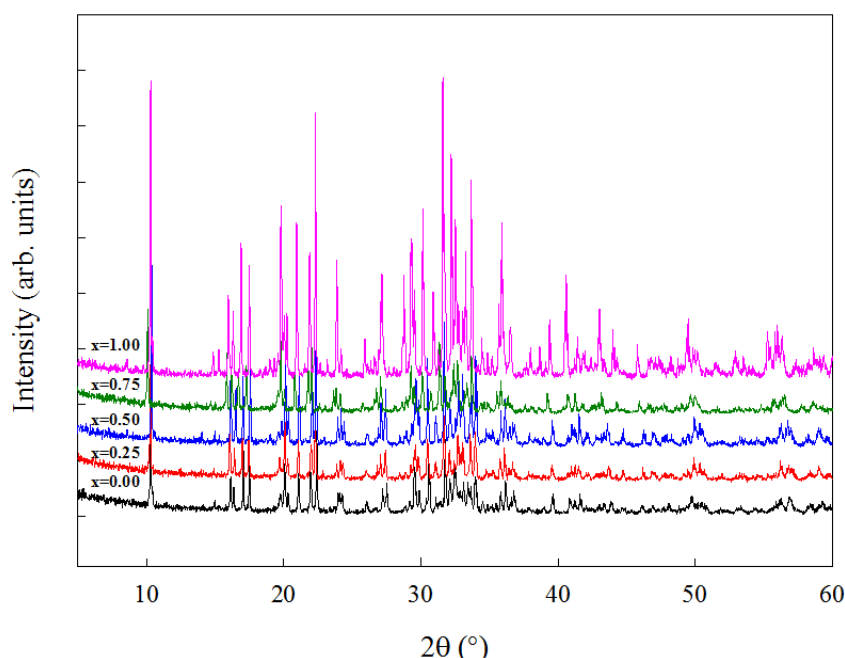


Figure 2. X-ray powder diffraction (XRPD) patterns of the Na₂Fe_{1-x}Mn_xP₂O₇ series.

Le Bail fitting was performed on all the patterns to derive unit cell parameters and volume; an example of such refinement is presented in Figure 3 for the $\text{Na}_2\text{Fe}_{0.5}\text{Mn}_{0.5}\text{P}_2\text{O}_7$ composition. Figure 4 shows the evolution of the unit cell volume along with the composition for the $\text{Na}_2\text{Fe}_{1-x}\text{Mn}_x\text{P}_2\text{O}_7$ series while in Table 1 the cell parameters are reported. This graph is indicative of the formation of a solid solution, with negative deviation from ideal Vegard law behavior. The calculated unit cell volume for the $\text{Na}_2\text{MnP}_2\text{O}_7$ end-member is in excellent agreement with values previously reported for this structure and composition [12,13]. The value obtained for the $\text{Na}_2\text{FeP}_2\text{O}_7$ end-member is in line with previous reports [12,14,17,18]. It should be recognized that a certain spread in volume parameters is observed in the literature for the Fe-based end-member, with values ranging from 570.66 \AA^3 [18] to 581.44 \AA^3 [14]. Variation in the unit cell volume for the same nominal composition may be indicative of the slight deviation from such nominal composition, in particular with regard to the exact Na content, which could be related to differences in synthetic procedure.

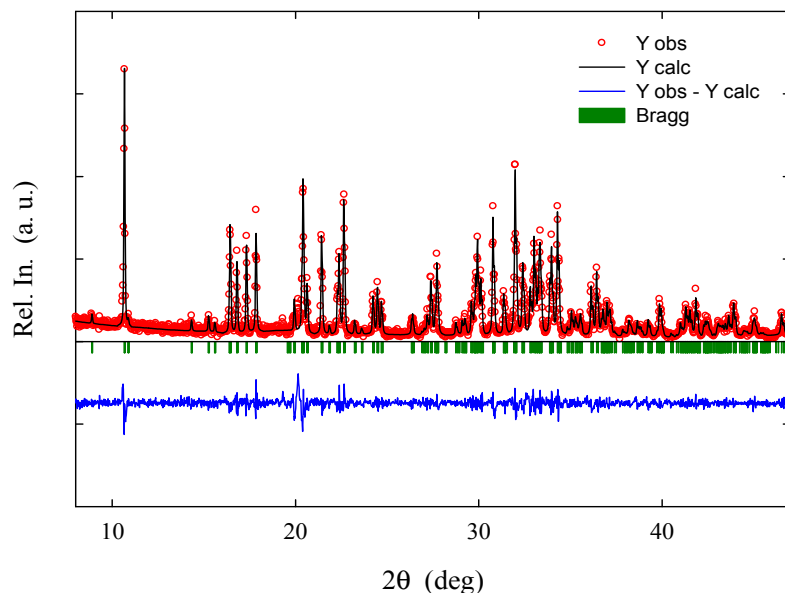


Figure 3. Example of LeBail fitting of the XRPD pattern of the $\text{Na}_2\text{Fe}_{0.5}\text{Mn}_{0.5}\text{P}_2\text{O}_7$ sample (χ^2 : 1.55).

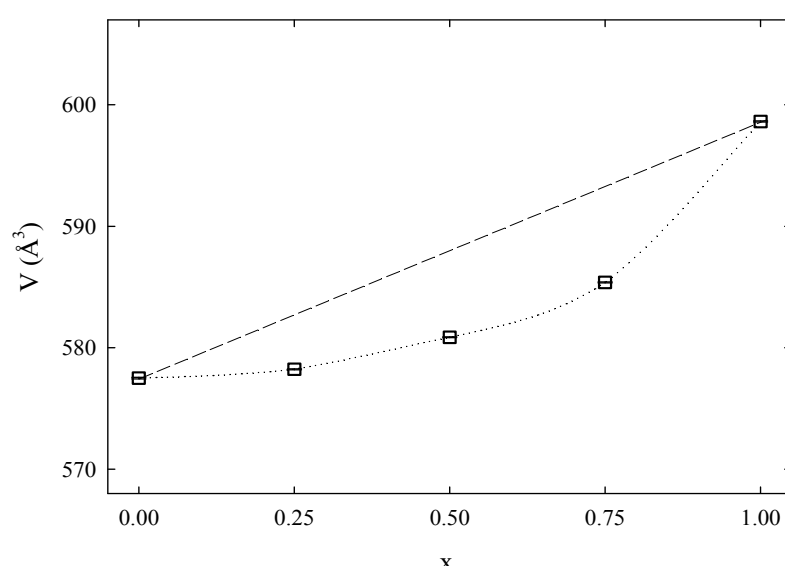


Figure 4. Unit cell volume as a function of x for the $\text{Na}_2\text{Fe}_{1-x}\text{Mn}_x\text{P}_2\text{O}_7$ series. Lines are guides for the eyes only. Standard deviations are within the size of the symbol.

Table 1. Cell parameters obtained from LeBail fitting of XRPD data for the $\text{NaFe}_{1-x}\text{Mn}_x\text{P}_2\text{O}_7$ series.

x	$a/\text{\AA}$	$b/\text{\AA}$	$c/\text{\AA}$	$\alpha/\text{deg.}$	$\beta/\text{deg.}$	$\gamma/\text{deg.}$	$V/\text{\AA}^3$
0	6.4431 (4)	9.4445 (6)	11.0014 (7)	64.639 (3)	85.689 (4)	72.978 (4)	577.46 (6)
0.25	6.4655 (1)	9.4550 (5)	11.0114 (4)	64.581 (4)	85.692 (6)	72.530 (3)	578.23 (7)
0.5	6.4824 (2)	9.4573 (3)	11.0545 (3)	64.207 (1)	85.458 (2)	72.749 (2)	580.86 (3)
0.75	6.5042 (3)	9.4676 (4)	11.0752 (5)	64.114 (2)	85.374 (3)	72.931 (3)	585.38 (4)
1	6.5608 (3)	9.5304 (2)	11.0964 (6)	64.101 (3)	85.699 (4)	73.329 (5)	598.13 (5)

SEM analysis shows that, on average, Mn-rich samples are characterized by larger grain dimensions (Figure 5). Such results are consistent with the higher thermal treatment necessary to achieve phase purity for $\text{Na}_2\text{MnP}_2\text{O}_7$ compared to $\text{Na}_2\text{FeP}_2\text{O}_7$ ($700\text{ }^\circ\text{C}$ versus $600\text{ }^\circ\text{C}$) and in line with the trend already observed in the literature for similar compositions [12].

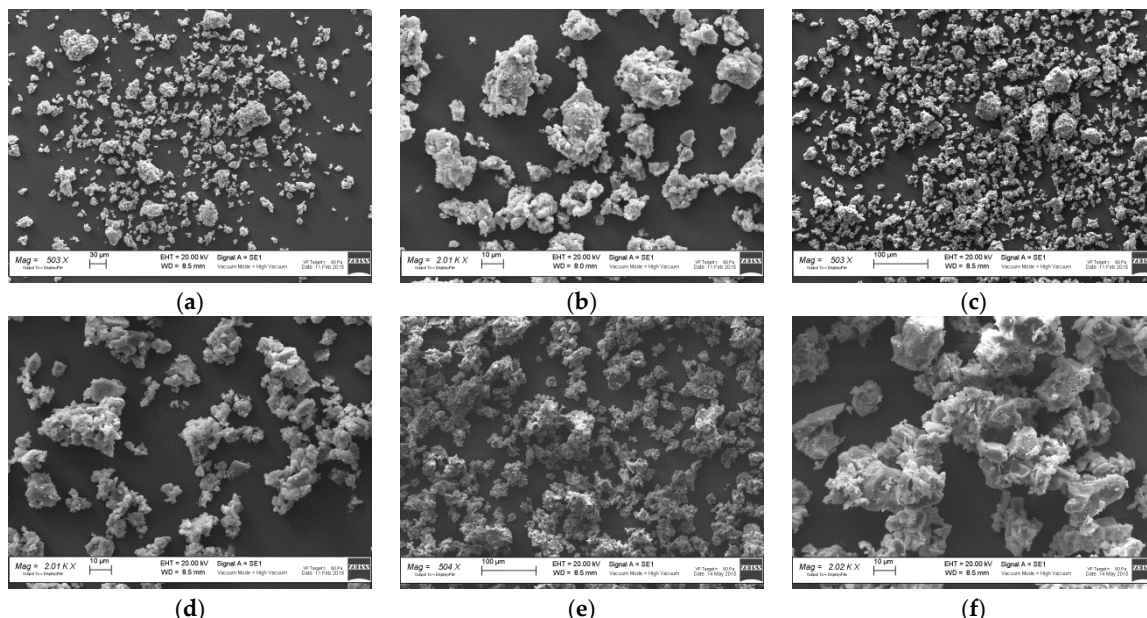


Figure 5. Scanning electron microscope (SEM) images at different magnification of (a,b) $\text{Na}_2\text{FeP}_2\text{O}_7$ powders; (c,d) $\text{Na}_2\text{Fe}_{0.5}\text{Mn}_{0.5}\text{P}_2\text{O}_7$ powders; (e,f) $\text{Na}_2\text{MnP}_2\text{O}_7$ powders.

In Figure 6, the SEM image and the maps of Mn and Fe obtained by the elemental microanalysis on the $\text{Na}_2\text{Fe}_{0.5}\text{Mn}_{0.5}\text{P}_2\text{O}_7$ sample are reported. It is evident that the distribution of both ions accurately reproduces the sample morphology. Thus, this technique supports the fact that, indeed, the two end-members form a solid solution of composition $\text{Na}_2\text{Fe}_{0.5}\text{Mn}_{0.5}\text{P}_2\text{O}_7$, rather than a two-phase mixture of compositions $\text{Na}_2\text{FeP}_2\text{O}_7$ and $\text{Na}_2\text{MnP}_2\text{O}_7$.

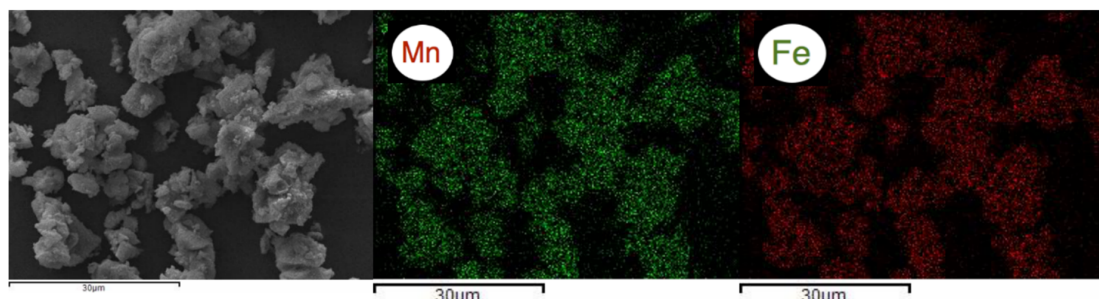


Figure 6. SEM-energy-dispersive X-ray spectroscopy (EDX) characterization of $\text{Na}_2\text{Fe}_{0.5}\text{Mn}_{0.5}\text{P}_2\text{O}_7$ showing the distribution of Fe and Mn within the powder sample.

All the samples in the $\text{Na}_2\text{Fe}_{1-x}\text{Mn}_x\text{P}_2\text{O}_7$ ($x = 0, 0.25, 0.5, 0.75, 1$) series were characterized for their electrochemical performances with standard half-cell assembly, as described in the Experimental Section. Figure 7 shows the CV curves in the potential range 1.5–4.0 V *versus* Na/Na^+ . The first information that can be extracted from these curves is that, under the experimental conditions used in this study, the CV response of the samples is strongly reduced as the Mn content increases, at the point that the electrochemical activity of pure $\text{Na}_2\text{MnP}_2\text{O}_7$ is barely observable, as previously reported for this system [12]. A decrease in electrochemical performances along with the substitution of Mn for Fe is common to other Mn-based polyanionic compounds, such as $\text{Li}_2(\text{Fe},\text{Mn})\text{P}_2\text{O}_7$ [23], and it has been generally attributed to the peculiar features of the $\text{Mn}^{2+}/\text{Mn}^{3+}$ redox couple, affected by large Jahn-Teller structural effects [13]. We recall here that the kinetics of sodium insertion/deinsertion is a very complex mechanism depending on several factors including lattice mismatch, low electronic conductivity, Jahn-Teller distortion, lattice strain upon intercalation/deintercalation, etc. Park *et al.* [13] proposed the degree of atomic rearrangement as a key metric for kinetic evaluation. In particular, structural rearrangements due to the accommodation of the Jahn-Teller distortion can provide a reference framework for the interpretation of noticeable differences in electrochemical behavior.

As it is possible to observe from Figure 7, for the $\text{Na}_2\text{FeP}_2\text{O}_7$ compound, the average voltages of the two major peaks are in fair agreement with those previously reported for this composition [14–16]. The shift in the average voltage as a function of composition is consistent with the trend observed for the two end-members, $\text{Na}_2\text{FeP}_2\text{O}_7$ [16] and $\text{Na}_2\text{MnP}_2\text{O}_7$ [13], where a shift of approximately 0.85 V was reported. Unfortunately, the very limited activity of $\text{Na}_2\text{MnP}_2\text{O}_7$ does not allow us to evaluate the absolute shift value between pure Fe and pure Mn in this study. We can presume that Fe-rich samples are characterized by a smaller shift in the voltage as Mn is introduced in the structure, whereas a more pronounced effect is expected for higher Mn contents ($x > 0.5$), as suggested by the difference between $\text{Na}_2\text{Fe}_{0.25}\text{Mn}_{0.75}\text{P}_2\text{O}_7$ (2.94 V) and $\text{Na}_2\text{Fe}_{0.50}\text{Mn}_{0.50}\text{P}_2\text{O}_7$ (2.72 V) compared to $\text{Na}_2\text{FeP}_2\text{O}_7$ (2.62 V) and $\text{Na}_2\text{Fe}_{0.75}\text{Mn}_{0.25}\text{P}_2\text{O}_7$ (2.65 V).

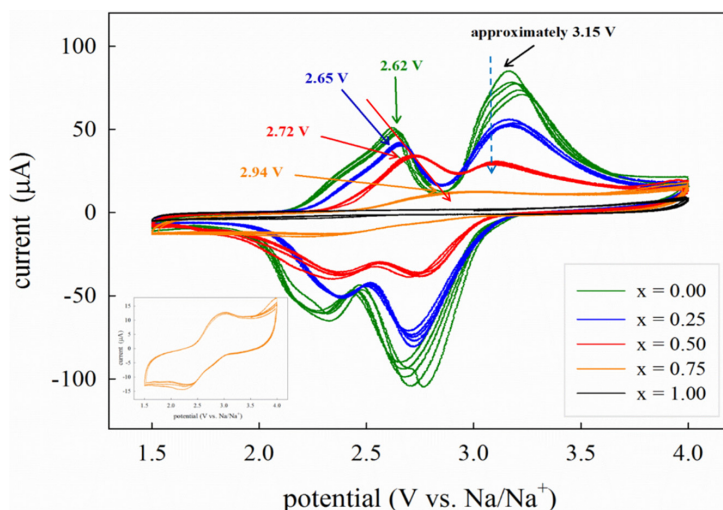


Figure 7. Cyclic voltammetry (CV) curves of the $\text{Na}_2\text{Fe}_{1-x}\text{Mn}_x\text{P}_2\text{O}_7$ series acquired at the scan rate of $0.1 \text{ mV} \cdot \text{s}^{-1}$. Inset: CV curve of the $x = 0.75$ sample in the range 1.5–4.0 V.

From Figure 7 it is also possible to note that, while for the peak centered at approximately 2.6 V a clear upward shift is detected along with increasing Mn content, the effect on the second part of the CV curve, centered around 3.15 V, is less pronounced. The reasons for such a behavior are unclear at the moment. The two regions of the CV curves have been associated with different electrochemical processes. In particular, the lowest potential peak, around 2.5 V for the $\text{Na}_2\text{FeP}_2\text{O}_7$ composition and around 3.3 V for the $\text{Na}_2\text{MnP}_2\text{O}_7$ composition, was identified as the result of a single phase reaction, while the second part of the curve, centered at approximately 3 V for $\text{Na}_2\text{FeP}_2\text{O}_7$ compound and above

4 V for $\text{Na}_2\text{MnP}_2\text{O}_7$, was attributed to different two-phase reactions [13,16]. From the present data, it can be inferred that the single-phase reaction process is sensitive to the nature of the metal cation, although it is possible that the second peak is also affected by the same voltage shift for higher Mn contents, but this is not visible in our case due to the low activity and the restricted voltage window used in these measurements, because of the electrolyte stability limit. Indeed, the CV profiles shown in a previous report of electrochemical activity for $\text{Na}_2\text{MnP}_2\text{O}_7$ were acquired up to 4.5 V and clearly showed, as visible in the inset of Figure 7, that the current was still increasing at such voltage [13]. We can also observe from Figure 7 that the shape of the CV curve for the $\text{Na}_2\text{FeP}_2\text{O}_7$ compound, as well as for the other compositions, is not as resolved as those previously reported in literature [16], in particular for what concerns the peaks around 3 V which, on the other hand, are attributed to less thermodynamically and kinetically favored two-phase transitions. This behavior may be due to several reasons: (i) the adopted scan rate that, as nicely shown in [16], is severely affecting the resolution of the CV curve, in particular for the high voltage region; (ii) the cathode microstructure (shape and size of particles) which, together with an efficient carbon coating, may strongly affect the kinetics of Na intercalation and de-intercalation in the system.

Figure 8 presents the charge/discharge cycles of the compounds of composition $\text{Na}_2\text{Fe}_{1-x}\text{Mn}_x\text{P}_2\text{O}_7$ ($x = 0.0; 0.25; 0.50$) at different C rates. At a given scan rate, the materials present a decreasing capacity as the Mn content increases. The most Mn-rich samples were not cycled as a consequence of the bad electrochemical activity presented in the CV curves. This worsening of the electrochemical properties is in line with what was previously reported for this system [12]. Overall, the capacity decreases when faster charge rates are used, as expected. However, a nice result is that the capacity is substantially retained over a certain number of cycles and the coulombic efficiency is almost 100% overall at higher current densities. Concerning the bad performances of the pure Mn compound, we stress that there is no full agreement in the literature. In particular, Barpanda *et al.* [12] reported bad properties for samples prepared by standard solid-state reactions. In contrast, Choi and co-workers [13] reported much better performances for samples subjected to ball-milling post-treatment for carbon coating. Since the morphology of the samples discussed in both the papers is similar, and is also similar to that of the present materials, we conclude that the optimization key in Mn (and even Mn-rich) pyrophosphates is a proper conductive coating able to counteract the intrinsic low electronic conductivity of these samples which is likely related to the electronic/structural features of the $\text{Mn}^{3+}/\text{Mn}^{2+}$ redox couple [13]. Indeed, a strong decrease of the particle dimensions can help to overcome this problem, as recently modeled for interphase electrochemical intercalation reactions [24].

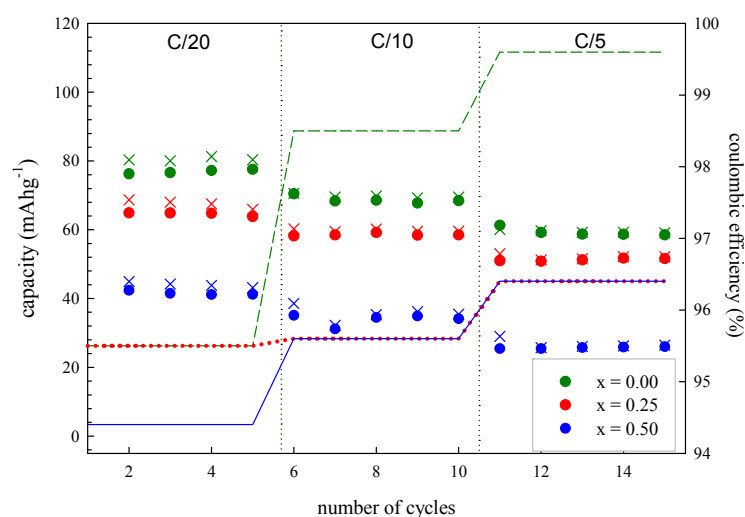


Figure 8. Charge/discharge plot for the $\text{Na}_2\text{Fe}_{1-x}\text{Mn}_x\text{P}_2\text{O}_7$ series ($x = 0.0; 0.25; 0.50$) at different charging rates in the 1.4–4.0 V range. Crosses indicate the charging process, points relate to the discharge process while lines indicate the coulombic efficiency.

4. Conclusions

In this study, the $\text{Na}_2\text{Fe}_{1-x}\text{Mn}_x\text{P}_2\text{O}_7$ solid solution was prepared by a conventional solid-state reaction and its electrochemical properties were investigated. The results presented here confirm that pure $\text{Na}_2\text{FeP}_2\text{O}_7$ and Fe-rich samples ($x = 0.75$) are promising cathode materials for application in sodium-ion batteries (SIBs), showing excellent columbic efficiency and high capacity compared to the theoretical one [14,18,19]. Mn-rich samples are instead not satisfactory, at least in the case of solid-state reaction recipes and standard slurry preparations, which is in agreement with previous reports [12]. By comparing our results with the previous literature, we infer that the peculiar nature of the $\text{Mn}^{3+}/\text{Mn}^{2+}$ redox couple may be partially responsible for the bad behavior of the Mn-rich samples compared to the Fe-rich phases. However, it is likely that the addition of carbon nanoparticles after material synthesis through solid-state reaction is not enough to assure high electrochemical activity, and better performances may be achieved through modification of the sample morphology and proper carbon coating.

Acknowledgments: Financial support from Fondazione Cariplo and Regione Lombardia through Project 2015-0753 is gratefully acknowledged.

Author Contributions: Cristina Tealdi, Eliana Quartarone and Piercarlo Mustarelli conceived and designed the experiments; Monica Ricci assembled the cells and performed the electrochemical tests; Chiara Ferrara prepared the samples and performed the XRD analysis; Giovanna Bruni performed the SEM experiments; Cristina Tealdi and Eliana Quartarone analyzed the data; Cristina Tealdi and Piercarlo Mustarelli wrote the paper.

Conflicts of Interest: The authors declare no conflict of interest.

References

- Yabuuchi, N.; Kubota, K.; Dahbi, M.; Komaba, S. Research development on sodium-ion batteries. *Chem. Rev.* **2014**, *114*, 11636–11682. [[CrossRef](#)] [[PubMed](#)]
- Kim, S.-W.; Seo, D.-H.; Ma, X.; Ceder, G.; Kang, K. Electrode materials for rechargeable sodium-ion batteries: Potential alternatives to current lithium-ion batteries. *Adv. Energy Mater.* **2012**, *2*, 710–721. [[CrossRef](#)]
- Xiang, X.; Zhang, K.; Chen, J. Recent advances and prospects of cathode materials for sodium-ion batteries. *Adv. Mater.* **2015**, *27*, 5343–5364. [[CrossRef](#)] [[PubMed](#)]
- Palomares, V.; Serras, P.; Villaluenga, I.; Hueso, K.B.; Carretero-Gonzalez, J.; Rojo, T. Na-ion batteries, recent advances and present challenges to become low cost energy storage systems. *Energy Environ. Sci.* **2012**, *5*, 5884–5901. [[CrossRef](#)]
- Palomares, V.; Casas-Cabanas, M.; Castillo-Martinez, E.; Han, M.H.; Rojo, T. Update on Na-based battery materials. A growing research path. *Energy Environ. Sci.* **2013**, *6*, 2312–2337. [[CrossRef](#)]
- Kubota, K.; Yabuuchi, N.; Yoshida, H.; Dahbi, M.; Komaba, S. Layered oxides as positive electrode materials for Na-ion batteries. *MRS Bull.* **2014**, *39*, 416–422. [[CrossRef](#)]
- Barpanda, P.; Nishimura, S.-I.; Yamada, A. High-voltage pyrophosphate cathodes. *Adv. Energy Mater.* **2012**, *2*, 841–859. [[CrossRef](#)]
- Sanz, F.; Parada, C.; Rojo, J.M.; Riuz-Valero, C.; Saez-Puche, R. Studies in tetragonal $\text{Na}_2\text{CoP}_2\text{O}_7$, a novel ionic conductor. *J. Solid State Chem.* **1999**, *145*, 604–611. [[CrossRef](#)]
- Erragh, F.; Boukhari, A.; Elouadi, B.; Holt, E.M.J. Crystal structures of two allotropic forms of $\text{Na}_2\text{CoP}_2\text{O}_7$. *Crystallogr. Spectrosc. Res.* **1991**, *21*, 321–326. [[CrossRef](#)]
- Erragh, F.; Boukhari, A.; Abraham, F.; Elouadi, B. The crystal structures of α - and β - $\text{Na}_2\text{CuP}_2\text{O}_7$. *J. Solid State Chem.* **1995**, *120*, 23–31. [[CrossRef](#)]
- Huang, Q.; Hwu, S.-J. Synthesis and characterization of three new layered phosphates, $\text{Na}_2\text{MnP}_2\text{O}_7$, $\text{NaCsMnP}_2\text{O}_7$, and $\text{NaCsMn}_{0.35}\text{Cu}_{0.65}\text{P}_2\text{O}_7$. *Inorg. Chem.* **1998**, *37*, 5869–5874. [[CrossRef](#)]
- Barpanda, P.; Liu, G.; Mohamed, Z.; Ling, C.D.; Yamada, A. Structural, magnetic and electrochemical investigation of novel binary $\text{Na}_{2-x}(\text{Fe}_{1-y}\text{Mn}_y)\text{P}_2\text{O}_7$ ($0 \leq y \leq 1$) pyrophosphate compounds for rechargeable sodium-ion batteries. *Solid State Ionics* **2014**, *268*, 305–311. [[CrossRef](#)]
- Park, C.S.; Kim, H.; Shakoor, R.A.; Yang, E.; Lim, S.Y.; Kahraman, R.; Jung, Y.; Choi, J.W. Anomalous manganese activation of a pyrophosphate cathode in sodium ion batteries: A combined experimental and theoretical study. *J. Am. Chem. Soc.* **2013**, *135*, 2787–2792. [[CrossRef](#)] [[PubMed](#)]

14. Barpanda, P.; Liu, G.; Ling, C.D.; Tamaru, M.; Avdeev, M.; Chung, S.-H.; Yamada, Y.; Yamada, A. $\text{Na}_2\text{FeP}_2\text{O}_7$: A Safe cathode for rechargeable sodium-ion batteries. *Chem. Mater.* **2013**, *25*, 3480–3487. [[CrossRef](#)]
15. Barpanda, P.; Ye, T.; Nishimura, S.; Chung, S.-C.; Yamada, Y.; Okubo, M.; Zhou, H.; Yamada, A. Sodium iron pyrophosphate: A novel 3.0 V iron-based cathode for sodium-ion batteries. *Electrochim. Commun.* **2012**, *24*, 116–119. [[CrossRef](#)]
16. Kim, H.; Shakoor, R.A.; Park, C.; Lim, S.Y.; Kim, J.-S.; Jo, Y.N.; Cho, W.; Miyasaka, K.; Kahraman, R.; Jung, Y.; *et al.* $\text{Na}_2\text{FeP}_2\text{O}_7$ as a promising iron-based pyrophosphate cathode for sodium rechargeable batteries: A combined experimental and theoretical study. *Adv. Funct. Mater.* **2013**, *23*, 1147–1155. [[CrossRef](#)]
17. Chen, C.-Y.; Matsumoto, K.; Nohira, T.; Ding, C.; Yamamoto, T.; Hagiwara, R. Charge-discharge behavior of a $\text{Na}_2\text{FeP}_2\text{O}_7$ positive electrode in ionic liquid electrolyte between 253 and 363 K. *Electrochim. Acta* **2014**, *133*, 583–588. [[CrossRef](#)]
18. Jung, Y.H.; Lim, C.H.; Kim, J.-H.; Kim, D.K. $\text{Na}_2\text{FeP}_2\text{O}_7$ as a positive electrode material for rechargeable aqueous sodium-ion batteries. *RSC Adv.* **2014**, *4*, 9799–9802. [[CrossRef](#)]
19. Longoni, G.; Wang, J.E.; Jung, Y.H.; Kim, D.K.; Mari, C.M.; Ruffo, R. The $\text{Na}_2\text{FeP}_2\text{O}_7$ -carbon nanotubes composite as high rate cathode material for sodium ion batteries. *J. Power Sources* **2016**, *302*, 61–69. [[CrossRef](#)]
20. Barpanda, P.; Ye, T.; Avdeev, M.; Chung, S.-C.; Yamada, A. A new polymorph of $\text{Na}_2\text{MnP}_2\text{O}_7$ as a 3.6 V cathode material for sodium-ion batteries. *J. Mater. Chem. A* **2013**, *1*, 4194–4197. [[CrossRef](#)]
21. LeBail, A.; Duroy, H.; Fourquet, J.L. *Ab-initio* structure determination of LiSbWO_6 by X-ray powder diffraction. *Mat. Res. Bull.* **1988**, *23*, 447–452. [[CrossRef](#)]
22. Rodríguez-Carvajal, J. Recent advances in magnetic structure determination by neutron powder diffraction. *Phys. B Condens. Matter* **1993**, *192*, 55–69. [[CrossRef](#)]
23. Furuta, N.; Nishimura, S.; Barpanda, P.; Yamada, A. $\text{Fe}^{3+}/\text{Fe}^{2+}$ redox couple approaching 4 V in $\text{Li}_{2-x}(\text{Fe}_{1-y}\text{Mn}_y)\text{P}_2\text{O}_7$ pyrophosphate cathodes. *Chem. Mater.* **2012**, *24*, 1055–1061. [[CrossRef](#)]
24. Kalantarian, M.M.; Oghbaei, M.; Asgari, S.; Ferrari, S.; Capsoni, D.; Mustarelli, P. Understanding non-ideal voltagebehaviour of cathodes for lithium-ion batteries. *J. Mater. Chem. A* **2014**, *2*, 19451–19460. [[CrossRef](#)]



© 2016 by the authors; licensee MDPI, Basel, Switzerland. This article is an open access article distributed under the terms and conditions of the Creative Commons by Attribution (CC-BY) license (<http://creativecommons.org/licenses/by/4.0/>).